Urban Climate 24 (2018) 675–691

Contents lists available at ScienceDirect

Urban Climate

journal homepage: www.elsevier.com/locate/uclim

Energy and water budgets of asphalt concrete pavement under simulated rain events

Jean-Martial Cohard[a], Jean-Michel Rosant[b,c], Fabrice Rodriguez[b,d,*], Hervé Andrieu[b,d], Patrice G. Mestayer[b], Pierre Guillevic[e,f]

[a] Laboratoire d'étude des Transferts en Hydrologie et Environnement (LTHE), UMR CNRS 5564, Université J. Fourier, Grenoble, France
[b] Institut de Recherche en Sciences et Techniques de la Ville (IRSTV), FR CNRS 2488, Nantes, France
[c] Laboratoire de recherche en Hydrodynamique, Énergétique et Environnement Atmosphérique (LHEEA), UMR CNRS 6598, École Centrale de Nantes, France
[d] Laboratoire Eau & Environnement (EE), Département Géotechnique, Environnement, Risques naturels et Sciences de la Terre (GERS), Institut Français des Sciences et Technologies des Transports, de l'Aménagement et des Réseaux (IFSTTAR), Bouguenais, France
[e] Department of Geographical Sciences, University of Maryland, College Park, MD 20742, USA
[f] Terrestrial Information Systems Laboratory, NASA Goddard Space Flight Center, Greenbelt, MD 20771, USA

ARTICLE INFO

Keywords:
Urban hydrometeorology
Water and energy budget
Surface evaporation
Eddy-correlation
Scintillometry
Asphalt concrete surface

ABSTRACT

Urban areas are subject to high human pressure and forthcoming enhanced hydrologic and climatic risks due to both city development and climate change. An asphalt concrete parking lot was instrumented in Nantes, France, to quantify the energy and hydrological responses of the surface to simulated rainfalls. The surface fluxes (precipitation, evaporation, radiation exchanges, sensible heat convection and conduction, runoff) were measured in situ and used to close the water budget with residual closure errors lower than 10%, depending on the surface evaporation retrieval method. The latent heat flux estimated from scintillometry measurements provided a better water budget closure than the direct eddy-correlation measurements. Runoff was the primary component of the water budget and represented around 80% of the total precipitation, compared to 17% for surface evaporation. The scintillometry method provided water evaporation time series at a 1-min time scale during the experiment. These series were used to characterize the rapid changes in the hydrological and energetic budgets of the asphalt surface after a precipitation event. During the drying phase the surface evaporation was significantly active, yielding 80% of the turbulent fluxes with a Bowen ratio of 0.25.

1. Introduction

Urban areas concentrate a large portion of human activities that have an increasing impact on the environment due to population growth (Steffen et al., 2015). In particular, rising urbanization significantly modified the hydrological cycle and energy budget of the Earth surface, due to the urban canopy morphology and changes in land use and land cover modes. Due to the complexity and high variety of the urban fabrics, the assessment of environmental impacts, as well as the evaluation of urban planning scenarios and sustainable development in response to climate variability and change increasingly rely on numerical simulations. A large proportion of the urban areas consists of streets, sidewalks, parking lots, and roads, usually made from asphalt concrete pavement. It is therefore

* Corresponding author at: IFSTTAR – GERS/EE, Route de Bouaye, CS4, 44344 Bouguenais Cedex, France.
E-mail addresses: jean-martial.cohard@univ-grenoble-alpes.fr (J.-M. Cohard), jean-michel.rosant@sfr.fr (J.-M. Rosant), fabrice.rodriguez@ifsttar.fr (F. Rodriguez), herve.andrieu@ifsttar.fr (H. Andrieu), patrice.mestayer@orange.fr (P.G. Mestayer), pierreg@umd.edu (P. Guillevic).

http://dx.doi.org/10.1016/j.uclim.2017.08.009
Received 13 April 2017; Received in revised form 19 July 2017; Accepted 22 August 2017

critical to assess the water and energy budget of asphalt concrete surfaces.

Runoff on urban surfaces is the principal component of the water budget from urban areas. It is usually represented using empirical relationship based on physical initial losses and a constant runoff coefficient. But several studies showed that such parameterization cannot account for all the involved processes (Berthier et al., 1999; Berthier et al., 2004) and that losses through evaporation during frequent rainfall events on these surfaces can reach several millimetres (Gash et al., 2008; Ragab et al., 2003b) particularly on streets (Hollis and Ovenden, 1988; Ragab et al., 2003a; Ramier et al., 2011). Urban surfaces collect atmospheric particulate pollution and the removal by rainwater of this pollution, further conveyed to the catchment outlet by runoff water, is directly influenced by the hydrological cycle and the succession of the wetting–drying periods (Amato et al., 2010). Stream thermal pollution (Herb et al., 2008) is due to the release to runoff water during rainfall events of solar energy absorbed by urban surfaces over warm periods of time and it contributes to increasing the water temperature downstream from urban areas (Kim and Sansalone, 2008; Van Buren et al., 2000). Vice versa this process could also be a solution to a negative impact of urbanization since pavement watering is viewed as a technique to reduce the urban heat island (Kinouchi et al., 1997). A recent experiment has been conducted in Paris in real conditions to improve this technique and to assess its efficiency (Hendel et al., 2016). For these issues the coupled simulation of urban water and energy budgets over long time series would benefit from appropriate experiments, allowing a more detailed parameterisation of both evaporation and runoff losses on urban surfaces (Dupont et al., 2006; Lemonsu et al., 2007; Rodriguez et al., 2008).

Also, interactions between urban canopies and the lower atmosphere have impacts on both the dynamics of the atmospheric boundary layer, through the modification of the partition of latent and sensible heat (Dupont et al., 2006), and the water cycle, enhancing clouds and modifying rain production (Changnon, 1981; Rozoff et al., 2003).

In meteorological models, urban areas were traditionally represented as dry surfaces (i.e., impervious with no or limited infiltration and storage) with high Bowen ratios (Thielen et al., 2000) where rain water is rapidly absorbed by the drainage system (e.g., the gutters). In contrast, Oke (1979) already stressed the variability of urban Bowen ratio, from 1.5 in dry periods to 0.3 after rain events. More recently Ramamurthy and Bou-Zeid (2014) and Santamouris (2014) reported observations of low Bowen ratios for wet urban surfaces and green roofs. In the early development of urban surface energy budget (hereafter denoted SEB) models, rain water and latent heat were not considered or computed separately from the energy budget. Recent models include the influence of evaporation either by combining the water and energy budgets of pervious and impervious surfaces within a tiling approach or by juxtaposing models for the urban (impervious) surfaces and natural (porous and vegetated) areas (see reviews by Grimmond et al. (2010) and Grimmond et al. (2011)). These models are generally derived from physically-based Soil-Vegetation-Atmosphere (SVAT) schemes initially developed for natural areas. However, these models use sets of parameterisations that cannot be easily calibrated due to the difficulties of driving accurate measurements in urban sites and the lack of reliable ground observational networks. SVAT parameterizations are generally derived from isolated measurements at the local scale or on analogies with observations over non-urban sites. Furthermore, based on SVAT formalism, the transfer of energy and water follows a one-dimensional approach that may not be valid in heterogeneous urban environment. Improving our knowledge in this field is of prime importance to foresee and mitigate the climatological change impacts on the urban climate.

The "Role of covered surfaces in urban hydro-system processes" project (ROSURE experiment in 2001–2002 and HydroVille experiment in 2003–2004) was dedicated to the characterization of the water and energy transfer processes within urban canopies, by combining in situ and numerical experiments (Berthier et al., 2004; Dupont et al., 2006; Rodriguez et al., 2008), with emphasis on semi-impervious surfaces, such as roads, streets and parking lots with asphalt concrete pavement.

In this article, we present results from a ground-based experiment conducted in Nantes in June 2004 to describe the water and energy budgets of a homogenous urban area, i.e. a parking lot during and after artificial rain events. This field experiment is unique at this scale (> 1 m^2 and < 1 ha) and in controlled conditions, compared to previous campaigns led on heterogeneous areas: between others, Bubble in Basel (Rotach et al., 2005) or CLU-Escompte in Marseille (Mestayer et al., 2005; Lagouarde et al., 2006) were experiments dealing on energy budget only. The three main objectives of the study were:

- To identify and propose an optimized method to obtain closed energy and water budgets of a semi-impervious parcel at a realistic scale;
- To develop a quality-assessed data set allowing to test and validate urban SEB schemes and hydrological models – this data set is now available upon request to the corresponding author;
- To improve our understanding of the evaporation process and of the energy partition during fair weather showers events.

The methodological issues and the rationale of our study are presented in Section 2. The experimental design and the meteorological data appear in Section 3. Surface flux measurements and uncertainty estimates of energy and water budgets are presented in Sections 4 and 5, respectively. The rapid hydrological and energetic behaviour of the asphalt surface during simulated fair-weather showers is analysed in Section 6. Our results are further discussed in Section 7 and we present a few conclusions in Section 8.

2. Methodological issues and study rationale

The experiment performed in 2004 was devoted to the closure of the water and energy budgets of an asphalt parcel, by measuring or deriving the different fluxes at the surface. The theoretical instantaneous budgets of the water layer covering the measurement area are:

$$dh/dt = P(t) - R_R(t) - E_v(t) - I(t) \quad (1)$$

$$\rho_w Cp_w dT_w/dt = Rn(t) - G(t) - H(t) - LE(t) - Q_R(t) \quad (2)$$

where h is the height (m) and T_w the temperature (K) of the water layer, P, R_R, E_v and I are the precipitation, runoff, evaporation and infiltration rates ($mm{\cdot}h^{-1}$), respectively, ρ_w ($kg{\cdot}m^{-3}$) and Cp_w ($J{\cdot}kg^{-1}{\cdot}K^{-1}$) are water density and heat capacity, respectively, Rn the net radiation ($W{\cdot}m^{-2}$), G the soil heat flux ($W{\cdot}m^{-2}$) to the underlying ground layers by conduction, H and LE the sensible and latent heat fluxes ($W{\cdot}m^{-2}$) to/from the atmosphere by turbulent convection, respectively, and Q_R the flux of sensible heat removed away from the text area by runoff water ($W{\cdot}m^{-2}$). The water layer is assumed horizontally homogeneous. These two budgets are twinned since E_v and LE on the one hand, R_R and Q_R on the other hand are related by proportionality relationships.

The rain water returned to the atmosphere by surface evaporation E_v is one of the most difficult flux to evaluate experimentally at the proper time and space scales. A major source of uncertainty is the underestimation of the heat fluxes to the atmosphere by the measurements of the turbulent fluxes above the surface (Foken et al., 2011). Aerodynamic methods rely on Monin-Obukhov similarity theory (MOST) stating that within the atmospheric constant-flux layer the vertical turbulent flux $< w'A' >$ is equal to the surface flux for any transportable quantity A emitted by the surface (with no source in the air), such as sensible heat and water vapour over most bare and vegetated grounds. In $< w'A' >$ the brackets $< >$ indicate the time average and the $'$ indicates the fluctuation around the average as in $A(t) = < A > + A'$, while w is the vertical component of the wind velocity. MOST assumes flow stationarity and surface homogeneity – two assumptions that are usually not verified in urban areas – and is only valid over large homogeneous surfaces that are, strictly speaking, rarely observed in natural continental environments (Foken et al., 2006). Over open areas with low obstacles the method accuracy is sufficient to close correctly the energy budget at the condition that the source area of the turbulent fluxes, located at some distance upstream from the sensors, has the same behaviour as that of the radiation fluxes, located just under the sensors. However, most experimental studies conducted to characterize the boundary layer above urban canopies showed significant temporal and spatial variability of the energy flux partition (Grimmond and Oke, 2002; Christen and Vogt, 2004; Mestayer et al., 2005; Pigeon et al., 2007; Mestayer et al., 2011).

The most direct measurement technique for evaluating the turbulent fluxes to the atmosphere is the eddy-correlation (EC) method. This method is said “direct” because the fluxes are directly proportional to the covariances of the vertical wind speed component w and temperature and humidity signals, T and q respectively:

$$< w'T' >_z \approx (r_a Cp_a)^{-1} H(z); < w'q' >_z \approx E_v(z) = L_v{}^{-1} LE(z) \quad (3)$$

where L_v ($J{\cdot}kg^{-1}$) is the latent heat of evaporation, ρ_a ($kg{\cdot}m^{-3}$) and Cp_a ($J{\cdot}kg^{-1}{\cdot}K^{-1}$) are air density and heat capacity, respectively. This method is most often implemented with a three-dimensional sonic anemo-thermometer (providing w' and T') associated to a fast-response hygrometer (providing q'). In the urban environment a further issue for the assessment of a small area surrounded by different surface types and obstacles is the sensor positioning. The sensors must be installed altogether high enough above the ground to be within an atmospheric layer where the turbulent vertical fluxes are close to the surface fluxes, and sufficiently low that the measured fluxes are always issued from a source within the surveyed area. The minimum and maximum appropriate heights depend on the surface roughness length, the distance between the sensors and upwind border of the measurement area and the wind speed, that varies in time. Finding the proper sensor position for an urban surface of limited area is a difficult task that may even appear impossible.

In this study, we developed the experimental design and methodologies adapted to the characterization of the various surface fluxes. A particular attention has been paid to address scale issues when attempting to close the budgets. Several hypotheses may explain the imbalance of the energy budget based on the turbulent flux measurements at low level (Foken et al., 2011), but there is no consensus about the final corrections that should be applied. In view of the remaining uncertainties on the evaporation rate E_v obtained with the EC method, in the present program we explored several alternative methods adapted to the monitoring of a small urban area, several of which (e.g., gradients, profiles) were not efficient. First, we implemented the EC method using sonic anemometers and KH20 hygrometers. Secondly, we tested an indirect method using a small aperture scintillometer to evaluate the spatially integrated sensible heat fluxes and derive the latent heat flux $Lv\ Ev$ from the residual of the energy budget (the other terms were measured by radiometers and thermometers. Ground heat flux and energy storage in infrastructures are generally not measured at urban sites but estimated as the residual of the energy balance equation (Christen and Vogt, 2004; Mestayer et al., 2005; Lagouarde et al., 2006; Pigeon et al., 2007). In this study we paid a great attention at the evaluation of this term, comparing several methods (see 4.2). In the rest of this article we compare the direct EC method and the indirect energy-budget residual method and assess their reliability and precision.

3. Experimental set up and meteorological conditions

The field campaign was conducted from May 29 to June 19, 2004. A clear sky period was chosen to benefit from high heat fluxes conditions. The study site was a parking lot located within the IFSTTAR institute at Bouguenais (47°9.3′ N, 1°38.95′ W) close to Nantes, France. About 60 km far from the Atlantic coast, this site is under the meteorological influence of the ocean but far enough to be never influenced by coastal breezes.

The instrumented area consisted of a 50 m × 50 m flat bare asphalt square (Fig. 1). It was equipped with a sprinkler network supplied by a hydraulic pump delivering up to 40 $m^3\,h^{-1}$ which was able to simulate precipitation events with intensities up to 16 $mm\,h^{-1}$. The surrounding areas remained dry during the simulated showers. Such micro-meteorological condition might generate

Fig. 1. View of the experimental site during a simulated rain event. The north is on the right.

a cool island and create divergent fluxes close to the ground during the spraying, as experienced by the participants standing at the border of the wetted area. Since the diverging flow ended immediately after the end of the sprinkling it was not considered in the analysis. The surrounding environment consisted of a low-tree forest 100 m far to the west (Fig. 1) and one tree row 100 m far to the north. The measurement area was also 50 m far from a building to the south-east, but it was never downwind from this building, nor in its shade. The instrumented area represented a catchment (surface area $S = 2500\ m^2$) whose outlet was equipped with a manhole (Fig. 2).

Characteristics of the instruments are summarized in Table 1. The simulated rain flow rate P was measured by a flowmeter at the pump. In addition, within a 500 m circle around the measurement site two rain gauges were monitoring natural rains. The spatially integrated runoff R_R at parcel scale was measured through a V-notch weir installed in the outlet manhole. The water temperature was measured by thermocouples at the pump and at the outlet. Percolation and soil water storage were monitored at the point scale and evaluated at parcel scale by means of borehole piezometers and humidity profiles.

The structure of the parking lot was composed of a 5 cm thick layer of asphalt concrete pavement above an old filled ballast layer characterized by a very low porosity. A heat plate and multiple series of thermocouples were installed in the soil to measure the temperature profile at depths from -1 to -75 cm (Fig. 2). In addition, 4 thermocouples were set to measure the surface temperature; infrared radiometer measurements were done in order to verify the impact of solar radiation and the accuracy of this measurement was good ($\pm$ 0.5 K). Radiation and meteorological variables were measured at 1 and 2 m above the surface (Table 1).

Two different sensor systems were used for measuring the sensible heat flux and the water vapour/latent heat flux. The first one consisted in two identical packages composed of a sonic anemo-thermometer and a fast open-path hygrometer operated at 1 and 2 m above the ground using the EC method. The second one was a small aperture scintillometer set at a height of 1.2 m for measuring the average sensible heat flux over a 70 m long diagonal transect (Fig. 2).

Positioning these sensors was critical (see Foken et al. (2011)). The sensor heights were derived from a sensitivity analysis of the

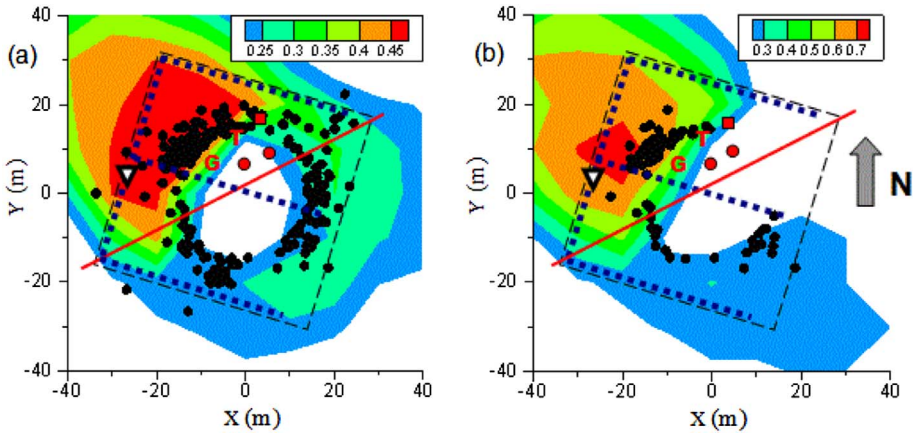

Fig. 2. Sketches of the measurement site showing the sprinkled measurement square (dash line), the sprinkler system (dotted blue lines), the scintillometer beam (red line), the two eddy-covariance sensor sets (red dots), the meteorological station (red square), the outlet manhole (white triangle), the ground heat flux plate (G), the thermocouple sets (T); the colours show the occurrence probabilities of the source function (80% contributions) of the eddy covariance measurements at 2 m, with the location of the individual 15 min maxima (black dots), for the entire data set (a) and for the ensemble of 3-h drying periods after rain events (b). (For interpretation of the references to colour in this figure legend, the reader is referred to the web version of this article.)

Table 1
Characteristics of the micrometeorological sensors (the variables are defined in the text).

Budget component	Instrument type	Number	z (m)	Measured variable	Time step
Radiation	CM6B (Kipp & Zonen)	2	1	$K\downarrow$, $K\uparrow$	1 min
	CGR3 (Kipp & Zonen)	2	1	$L\downarrow$, $L\uparrow$	
Net radiation	NRlite (Kipp & Zonen)	1	1	Rn	1 min
Sensible heat flux	Sonic Anemometer USA1 (Metek)	2	1 and 2	u^*, $< w'T' >$	0.1 s
	Scintillometer SLS20 (Scintec)	1	1.2	C_n^2, C_T^2, l_o, u^*_{SLS}, H_{SLS}	1 min
Latent heat flux	KH2O (Campbell Sci)	2	1 and 2	$< w'q' >$	0.1 s
Surface temperature	Thermocouples	4	0	T_s	60 s
Ground heat flux	Flux meter HFP01 (Huskflux)	1	− 0.03	G	1 min
	Thermocouples	32	0 to − 0.75	T(z)	1 min
Meteorological parameters	Wind monitor (Young)	1	1.5	U, Wind dir	1 min
	HMP45C (Vaisala)	2	1 and 2	T, RH	1 min
	Rain gauges (Precis Mecanique)	2	1.2	P	1 min
Water flow	Sprinkler flowmeter (Schlumberger)	1	/	P	1 min
	Pressure sensor (Druck)	1	0	h, R_R	1 min
	Thermocouples	2	1.2, 0	T_{wP}, T_{wR}	1 min

footprint model developed by Schmid and Oke (1990) to verify the criteria given in Section 2: (i) high enough above the ground to be within a layer where the turbulent vertical fluxes were close to the surface fluxes and (ii) sufficiently low that the measured fluxes were always issued from a source area within the sprinkled zone. The measurement quality also required that the EC sensor height was at least one order of magnitude larger than their spatial resolution. Since the sonic sampling resolution was about 10 cm, the minimum height was estimated about 1 m. A higher sensor was expected to sample a larger footprint, providing a better statistical representativeness but at the risk of being contaminated by sources outside of the experimental square. Results for the 2 m high sensor (Fig. 2) show that (i) the maximum of the footprint function was always located within the asphalt area and (ii) the probability that 80% of the flux contributions were issued from the measurement square was of 45% for the whole data set and 70% for the data obtained during the showers and drying periods. Similar results for the scintillometer (not shown) indicate that the criteria were also verified at 1.2 m.

During the month of June 2004, the meteorological situation was favourable with low wind conditions. After the 1st of June, the region was under the influence of an anticyclone yielding winds from the northwest ($\approx 300^\circ$) at the beginning of the experiment. Due to the anticyclonic centre displacement, the synoptic wind turned to the east from June 5–6, veered from 60° to 300° between June 7 and 10 and remained weak (< 3 m s^{-1}) from the northwest until the end of the campaign. Only one natural rain was observed on June 10 at 12:30, and a short drizzle during the night of June 8–9, associated with some nebulosity in the morning (Fig. 3b, c). The other days of the period were characterized by sunny conditions with rare cumulus. The surface temperature remained always higher than the air temperature, even at night by at least 3.75 K and up to 23.3 K at mid-day (Fig. 3a). The ramps of the sprinkling system were adjusted on June 3 and 4 to ensure that all the water fell within the instrumented squared area. Afterwards two simulated rain events, hereafter called showers, were performed each day from June 7–11 at different times in the morning and in the afternoon after the asphalt had completely dried out. The showers lasted 20 to 40 min and the drying period varied according to the radiation conditions. On June 9, an additional shower was performed at 15:40 before the surface completely dried from the preceding event of 13:40, but this event was designed very short and produced very little runoff.

June 6 was a cloudless day with no rainy event that was especially convenient for assessing the energy balance closure because of the very steady conditions of eastern wind. It appears in the following time series as a reference day without rain event.

4. Energy budget results and assessment

The instantaneous budget Eq. (2) must be integrated in time and space over the measurement square to describe the experimental energy budget of the water layer above the asphalt area:

$$Rn \approx G + Q_R + H + LE + X \tag{4}$$

where the brackets are omitted for simplicity. The last term X is the residual from the energy balance as described by Foken et al. (2006). It includes measurement errors and may also include energy accumulation/storage in the atmospheric layer between the water surface and the sensors due to horizontal advection (Foken et al., 2006). Since this atmospheric layer is thin the imbalance term X is expected to remain small and to converge towards zero at large time scales. For the sake of clarity, Eq. (4) is called the SEB equation hereafter. In the following sub-sections, we analyse the optimal method to derive each of the SEB terms for our study site.

4.1. Net radiation measurements

Since the atmospheric layer between the radiometers and the ground is very thin Rn(z) is close to the net radiation at the surface, commonly expressed as the result of the radiation budget:

$$Rn = K_\downarrow - K_\uparrow + L_\downarrow - L_\uparrow \tag{5}$$

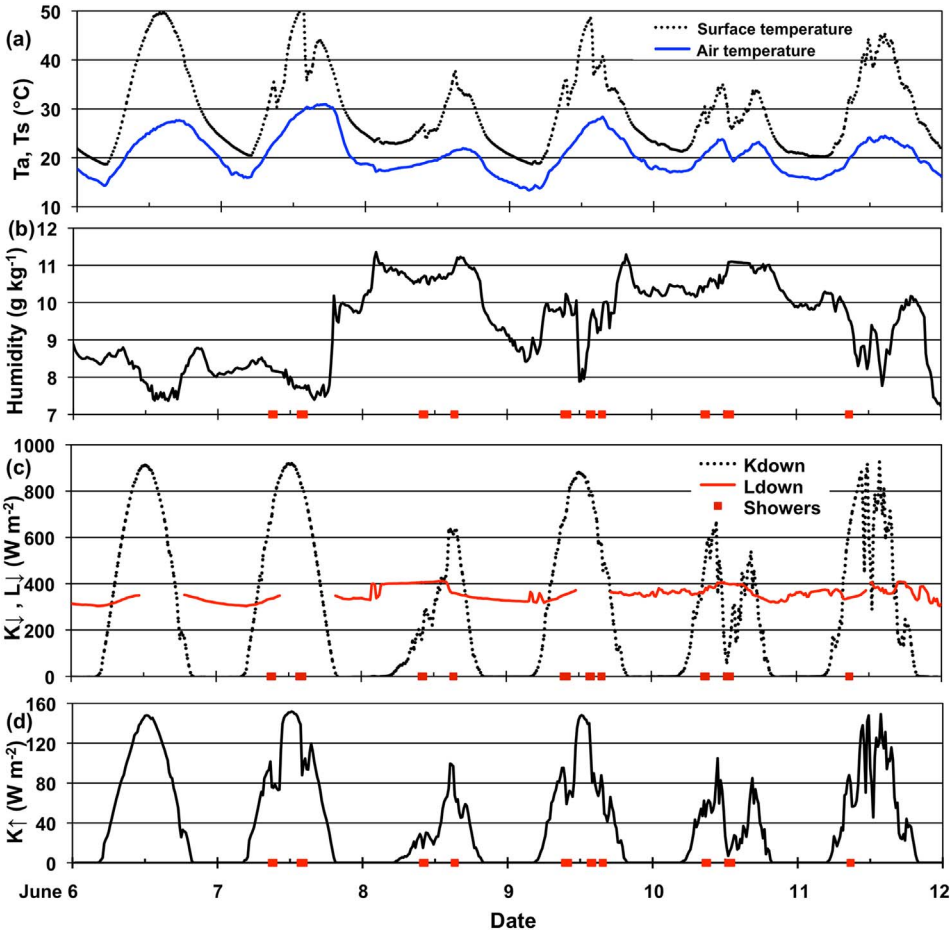

Fig. 3. Time series of air (solid line) and surface (dotted line) temperatures (a), specific humidity (b), downward solar (dotted line) and longwave (solid line) radiations (c), upward radiation (d) during the analysed period (June 6–11). The red dots indicate rain events. The abscissa main tics correspond to 00:00 UTC and the secondary tics to 12:00 UTC. (For interpretation of the references to colour in this figure legend, the reader is referred to the web version of this article.)

where $K_{\downarrow}$ and $K_{\uparrow}$ are the downward and reflected shortwave radiations, respectively, $L_{\downarrow}$ and $L_{\uparrow}$ the incoming and upcoming longwave (thermal infrared) radiations ($W{\cdot}m^{-2}$), respectively. Each of the four radiative components were measured separately and the net radiation was independently measured by a net radiometer (Table 1). All radiation sensors were cleaned up immediately after each sprinkling to remove the residual water. The surface albedo, defined as the ratio $K_{\uparrow}/K_{\downarrow}$ was about 0.17 for the asphalt concrete was dry and it dropped to 0.10 when the surface was covered by the water layer. Direct measurements of $L_{\uparrow}$ combined with surface temperature T_s from the thermocouples were used to evaluate the surface emissivity ε_s, using the Stefan-Boltzmann law $L_{\uparrow} = \sigma\,\varepsilon_s\,T_s^4$ where σ is the Stefan-Boltzmann constant ($\sigma = 5.67\ 10^{-8}\ kg\ s^{-3}\ K^{-4}$). The derived emissivity ε_s (−) was 0.93 for dry conditions and 1.0 for wet conditions. Reciprocally we used the surface temperature measurements and Stefan-Boltzmann law to complete the missing longwave data of June 6 and 7.

The showers have significant impacts on the surface temperature T_s and reflected solar radiation $K_{\uparrow}$ (Fig. 3a, d). Rapid and strong surface temperature drops (up to 13 K) were observed during the simulated showers (Fig. 3a). Time series of net radiation derived from the net radiometer and from the four components of the radiative budget (Eq. (5)) are in very good agreement (Fig. 4). The correlation between the two time series is excellent: the linear regression yields a slope of 1.05 and a coefficient of determination R^2 of 0.99. Nevertheless, the supplemented estimation of the net radiation from the four components was preferred to that of the net radiometer since the NR-Lite radiometer seemed to underestimate the longwave contribution as shown during the nights in Fig. 4. Moreover, the NR-Lite radiometer appeared sensitive to rain and did not provide data during and immediately after rainfalls.

4.2. Ground heat flux measurements

The soil heat flux was estimated using two different methods. The first method was based on measurements from a ground heat plate installed 3 cm under the surface. They were corrected for the energy storage between the sensor and the surface using the approach proposed by Anandakumar (1999) and Braud et al. (1993). The second method was based on the temperature measurements with thermocouples in the ground, using the harmonic method initially developed by Van Wijk and De Vries (1963) and

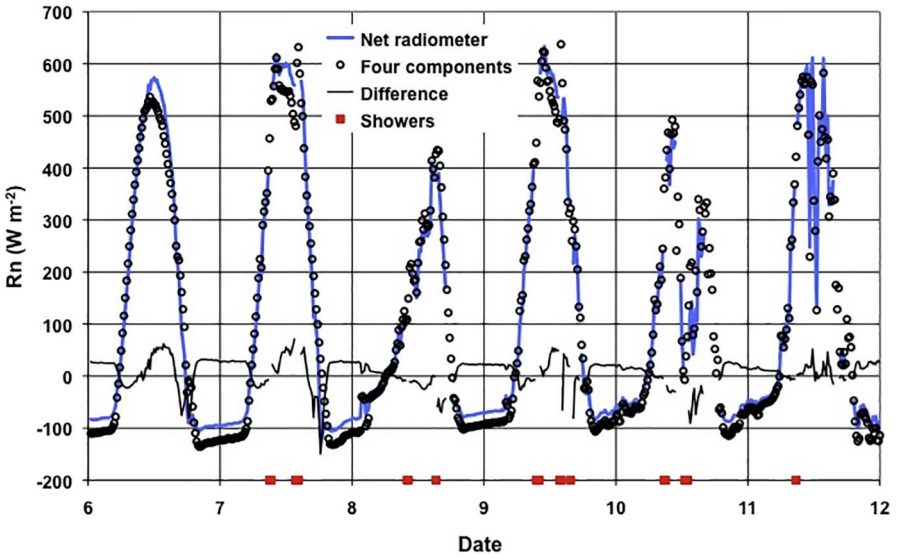

Fig. 4. Time series of the net radiation from the measurements of the net radiometer (solid blue line), the four radiative components using Eq. (5) (symbols) and their difference (thin black line). (For interpretation of the references to colour in this figure legend, the reader is referred to the web version of this article.)

refined by Heusinkveld et al. (2004) and Verhoef (2004).

A Fourier series decomposition of the temperature time series T_{ref} measured at depth z_{ref} provides an analytical solution T_F (z_G, t) of the heat diffusion equation $\partial T/\partial t = \alpha_T \partial^2 T/\partial z^2$, at any depth z_G and any time t as well as its vertical gradient (Eqs. (6) and (7)).

$$T_F(z_G, t) = \sum_k 2C_k \exp\left(-\frac{z_G}{z_\alpha}\right) \sin\left(\omega_k t + \varphi_k - \frac{z_G}{z_\alpha}\right) \tag{6}$$

$$\frac{\partial T_F}{\partial z}(z_G, t) = \sum_k \frac{2\sqrt{2}\,C_k}{z_\alpha} \exp\left(-\frac{z_G}{z_\alpha}\right) \sin\left(\frac{\pi}{4}\omega_k t + \varphi_k - \frac{z_G}{z_\alpha}\right) \tag{7}$$

C_k and ϕ_k are the norm and phase of the kth complex Fourier coefficient, respectively, ω_k the period of the kth harmonic, $\omega_k = 2\pi\, k\, N^{-1}\, \delta t$, N the total number of data considered in the Fourier analysis, δt their time step, and z_α a diffusion equivalent depth, $z_\alpha = (2\ \alpha_T\ \omega_k{}^{-1})^{1/2}$ where α_T is the heat diffusion coefficient of the ground surface layer. The heat flux at the surface is therefore obtained from Eq. (8).

$$G_F = \rho_d Cp_d \alpha_T \frac{\partial T_F}{\partial z}\,|_{z_G=0} \tag{8}$$

where ρ_d (kg·m^{-3}) and Cp_d (J·kg^{-1}·K^{-1}) are the dry density and heat capacity of the ground surface layer, respectively. The reference temperature T_{ref} was computed by averaging four measurements at the depths of 1 and 2 cm, using z_{ref} = 1.5 cm. Average values were used to minimize measurement spatial variability due to asphalt concrete heterogeneity since an error of a few mm in thermocouple depth might induce large differences in the temperature time series.

The heat diffusion coefficient α_T was computed from the temperature measurements at z_G = 0 cm and z_G = 1.5 cm using the amplitude method developed by Verhoef et al. (1996) based on an analytic resolution of the conductive heat transfer equation using a Fourier series representation of temperature. The average value over the whole measurement period was found to be α_T = 1.16 10^{-6} m^2 s^{-1}. It is supposed to vary with the different layers of the parking lot structure. However, this was not observed on Fig. 5, which shows that the phase shift increased linearly with depth until 24 cm. this linear phase shift was clearly broken between − 24 cm and − 50 cm. In the following we considered a constant diffusion coefficient between 0 and − 24 cm.

The temperatures $T_F(z_G)$ obtained with the Fourier model for z_G = − 1.5 cm were in very good agreement with the measured temperatures T_m at z = − 1.5 cm with a coefficient R^2 > 0.999 and no bias. The ability of the method to reproduce the signal at other depths was also demonstrated by the model-to-measurement linear regressions for $z_G = z$ = 0 and − 5 cm: T_F = 0.98 T_m + 0.88 with R^2 = 0.996 and T_F = 0.99 T_m + 0.38 with R^2 = 0.998, respectively. The performance of the model was slightly reduced for the surface temperature due to the strong impact of the shower periods.

The ground heat flux at z = 0 was obtained using Eq. (8) with ρ_d = 2050 kg·m^{-3} and Cp_d = 920 J·kg^{-1}·K^{-1} for the dry asphalt concrete, taken from the literature (Incropera et al., 2006) and comparable with other studies dealing with asphalt thermal properties (Chadbourn et al., 1996; Mrawira and Luca, 2006). The effect of humidity on these properties was not taken into account because of near-zero porosity of asphalt concrete. We compared the ground heat flux derived from the Fourier analysis method G_F (Eq. (8)) to the measurements with the heat plate at a 3-cm depth before (G_{HP}) and after (G_{HPC}) correction for the heat stored in the 3-cm thick soil layer between the surface and the sensor (Fig. 6). The G_F and G_{HPC} time series were very well correlated (R^2 = 0.98) but we

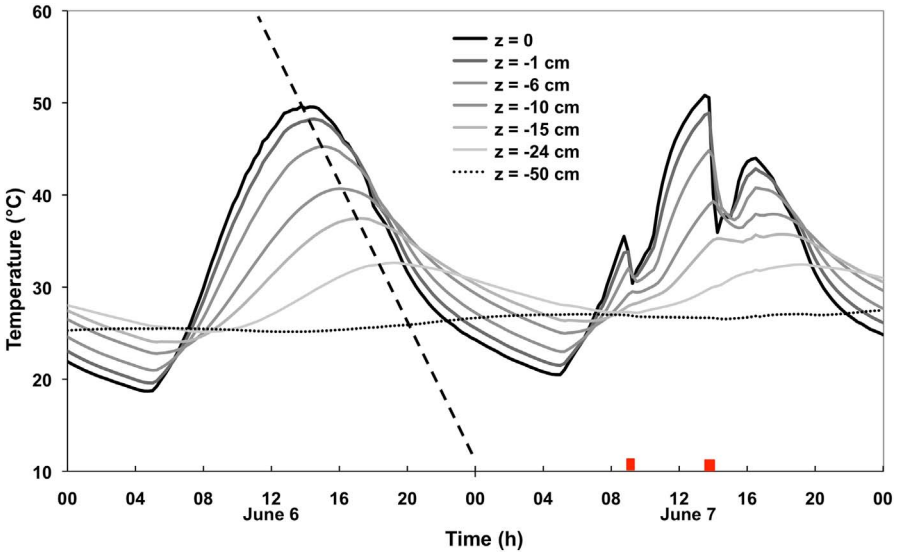

Fig. 5. Soil temperature time series for June 6 (no rain) and 7 (two rain events). The dash line shows the linear time lag dependence with depth and the red dots indicate the simulated showers. (For interpretation of the references to colour in this figure legend, the reader is referred to the web version of this article.)

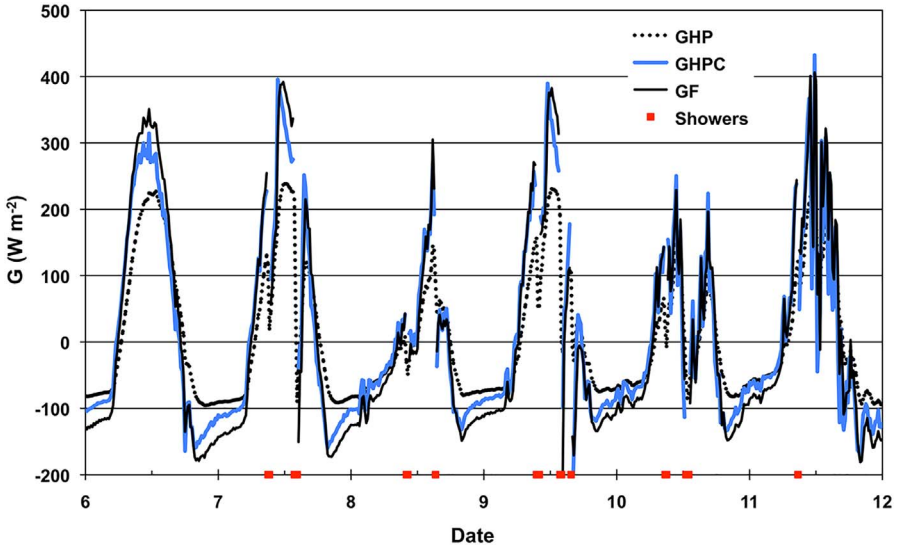

Fig. 6. Comparison of ground heat fluxes obtained with the Fourier analysis method G_F (solid line), the raw measurements with the heat flux plate at $z = -3$ cm G_{HP} (dotted line) and the measurement corrected for the energy stored between the plate and the surface G_{HPC} (grey line).

observed that results from the harmonic method were slightly higher and the associated linear regression was $G_F = 1.087\ G_{HPC} - 6.5$. Harmonic method estimated values have been removed during rain events because they are affected with large uncertainties and not necessary for further calculation (see the gaps in Fig. 6). Indeed, the sharp change in near surface temperature when rainfall reach the ground is produce high frequencies in the harmonic method which are not well solved with the available data.

Thereafter, we used the ground heat flux estimates derived from the harmonic method for mainly two reasons: (i) flux estimates were based on measurements from thermocouples that are more reliable sensors than the flux plate; (ii) these estimates provided a better closure of the energy budget at night when the heat conduction in the ground was essentially balanced by the infrared radiation (night-time sensible heat flux was lower than 40 W m^{-2} and sometimes negative).

The ground heat flux G is one of the major terms of the SEB equation and represents up to two thirds of the net radiation Rn. The asphalt layer was storing a significant amount of energy during the day that was available to provide either large night-time infrared flux (200 W m^{-2} at night, Fig. 6) or the required energy used to evaporate rain water, as shown by G rapid decreases after each shower (Fig.6).

4.3. Runoff heat flux

Runoff heat flux Q_R was calculated using the flow rate measured at the runoff water outlet R_R ($m^3\ s^{-1}$) and the difference between the water temperatures measured at the outlet T_{wR} and at the pump T_{wP}:

$$Q_R = \rho_w\ Cp_w\ R_R\ (T_{wR} - T_{wP}) \quad (9)$$

where the tap water temperature T_{wP} was actually constant throughout the campaign and equal to 18 °C, apart from June 10, where a natural rain occurred and this temperature was 21 °C.

The runoff water carried large instantaneous heat fluxes, varying from a few W m^{-2} for a natural rain up to a maximum of 438 W m^{-2} during some simulated showers. However, these large fluxes decreased significantly 15 min to 1 h after the end of the showers; as ($T_{wR} - T_{wP}$) does not vary too much during the rain event, this strong decrease is mainly related to the R_R runoff decrease (see Section 6 and Fig. 12).

4.4. Turbulent heat fluxes and surface energy balance assessment

4.4.1. Eddy-correlation measurements

With the EC method the sensible and latent heat fluxes are estimated from the covariances of the vertical wind speed component and temperature and humidity signals (Eq. (3)). Here, the covariances $< w'T' >$ and $< w'q' >$ were first calculated from the raw data and $< w'q' >$ was further corrected for the time lag between the sonic and hygrometer, using the delay that maximized the correlation between w(t) and q(t). Additional corrections included sonic temperature correction for humidity, specific humidity correction for oxygen, Webb corrections and frequency corrections accounting for high path and low path filters, sensor path averaging and sensor separation (Aubinet et al., 2012) using the EdiRe software (EdiRe). The corrected values of $< w'T' >_z$ were 7.5% higher and the corrected values of $< w'q' >_z$ 19% higher than the raw covariances, on average. The covariances were further averaged over 15 min.

The closure of the energy budget was assessed by evaluating the balance between the total turbulent heat flux (sensible plus latent) measured with the EC method and the total energy flux available at the surface for the 6-day period from June 6–12 (Fig. 7). In the dry situations with negligible latent heat ($LE < 50$ W m^{-2}, open symbols in Fig. 7), the total turbulent flux was relatively well correlated with the available energy flux $Rn - G - Q_R$. The scatter was relatively large with linear regression coefficients $R^2 = 0.68$ for the measurements at 1 m and $R^2 = 0.71$ at 2 m and slopes of 0.63 and 0.76, respectively. The total turbulent flux was 20% higher when measured at 2 m than at 1 m. Such a relative difference is important but must be put in perspective with observed large deviations (up to 100 W m^{-2}) and with relatively low values of the sensible heat flux (lower than 250 W m^{-2}). For dry conditions, the low values of the measured sensible heat flux confirmed the primary role of the conduction heat flux in the surface energy budget. For the wet conditions, Fig. 7 (solid symbols) shows also a large scatter of the energy balance, with the total turbulent flux lower than the available energy flux: the slope of the linear regressions were 0.74 for the measurements at 1 m and 0.76 at 2 m with R^2 coefficients of 0.67 and 0.29, respectively.

Results clearly showed that EC measurements were not able to close the energy budget (Eq. (4)), with an average imbalance of around 30% of the available surface energy for measurements at 1 m (slope 0.70, $R^2 = 0.85$) and 24% for measurements at 2 m

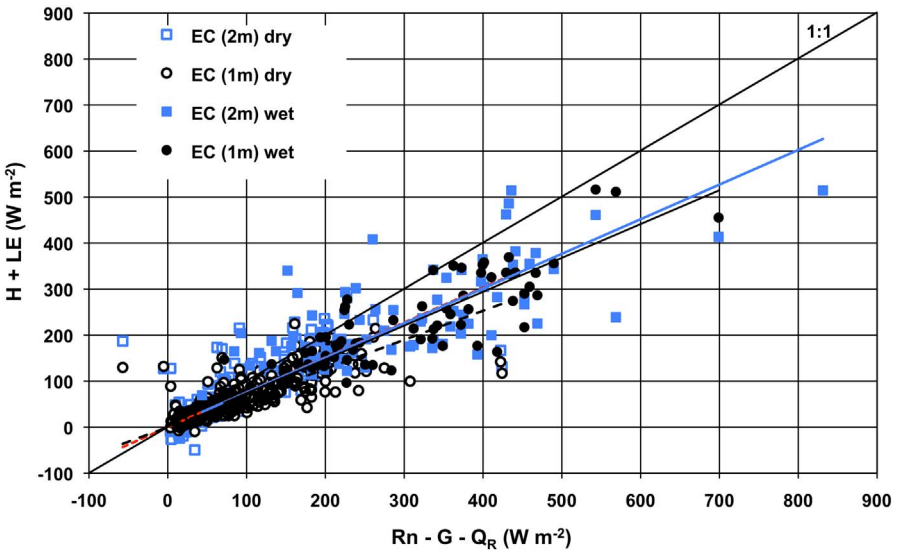

Fig. 7. Balance between the total energy flux available at the surface and the total turbulent heat flux measured at the heights of 1 m (circles) and 2 m (squares) in dry conditions (LE < 50 W m^{-2}, open symbols and dash lines) and wet conditions (solid symbols and lines); with the same slope the 2-m dry and wet regression lines are superimposed.

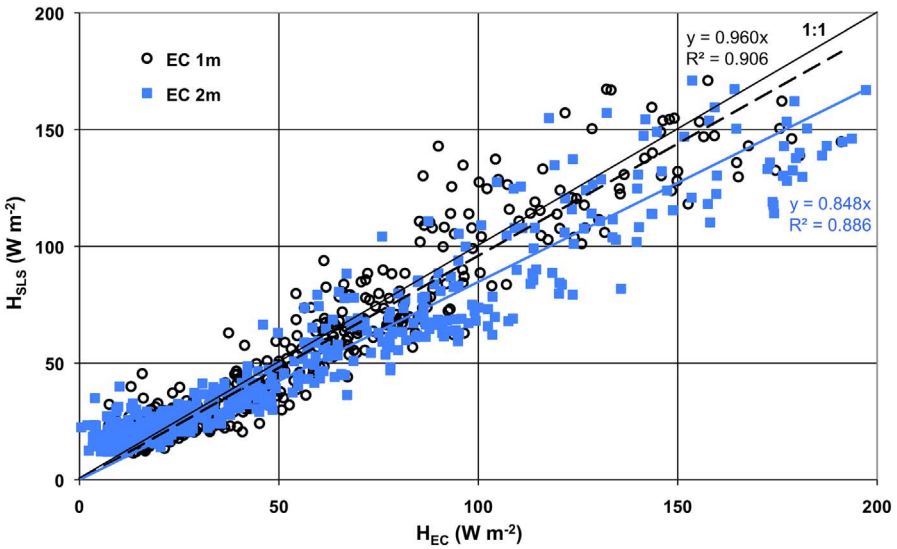

Fig. 8. Comparison of the sensible heat flux estimated from the scintillometer measurements and from the sonic anemometers at 1 m (black circles and dash line) and at 2 m (red squares and solid line). (For interpretation of the references to colour in this figure legend, the reader is referred to the web version of this article.)

(slope 0.76, $R^2 = 0.79$).

4.4.2. Estimations from the small aperture scintillometer

The second method used to estimate the sensible heat flux was based on measurements from the small aperture scintillometer with a path length of 70 m at 1.2 m above the ground. With the Scintec SLS20 scintillometer two parallel collimated laser beams were transmitted through the atmosphere and used to simultaneously obtain the momentum and sensible heat fluxes (Thiermann and Grassl, 1992).

Scintillometry consists in analysing the received fluctuating intensity of a light beam that encounters deviation and scattering by turbulent eddies. The variance of the received signal intensity logarithm is related to turbulence parameters averaged along the path between transmitter and receiver. The relationships that we used to derive the turbulent fluxes from scintillation measurements are presented in the Appendix and more details about the retrieval algorithm can be found in Hill (1992) for a review, Wheelon (2003) for the theory and Lagouarde et al. (2006) for urban measurements.

The sensible heat fluxes *H* derived from scintillometry were on average slightly lower than *H* measured with the EC method at 1 m and 15% lower than *H* measured at 2 m (Fig. 8). An overestimation is nevertheless apparent for the low values that may be attributed to an overestimation of the friction velocity (see Eq. (A.6) in the Appendix) in the near neutral conditions encountered at night (De Bruin et al., 2002; Hartogensis et al., 2002).

These comparisons show that the sensible heat flux estimated with the eddy covariance method was, after corrections, about 13% higher at z = 2 m than at 1 m, on average, because at 2 m the EC sensors capture turbulent eddies over a larger size range. However, as previously mentioned, the dispersion is important and the events are too brief for a spectral analysis that would confirm this hypothesis. Although, the footprint of the 2mEC measurement may include some dry surfaces, out of the watered parking lot, and consequently higher sensible heat fluxes. Moreover, the showers might generate a possible cool island above the asphalt area which might in turn induce some flux divergence for a while, increasing the budget unsteadiness with transient values of the unbalance term *X* (Eq. (4)).

In this second method, the latent heat flux *LE* was estimated from the closure of the energy budget (Eq. (4)), assuming that *X* was negligible. This assumption is rational because we considered that ground-based measurements were acquired with very low uncertainties: *H* was derived from scintillometry, *G* from the thermocouple measurements and the harmonic method, Q_R from the runoff water flow and temperature, and *Rn* from the four component radiometers. Results showed that the latent heat flux *LE* derived from this method were significantly higher than *LE* obtained with the EC method (Fig. 9). The slopes of the linear regressions between *LE* from the two methods were 1.25 and 1.13 for the EC measurements at 1 m and 2 m, respectively.

Time series of *LE* measured with the EC method and derived from the SEB method (Fig. 10) were used to evaluate the two methods and characterize the asphalt surface energetic response to rain events:

- The rapid response of the surface to simulated showers was represented by large positive peaks (the event of June 10 at 12:30 was a natural rain, see Fig. 10). The EC measurements were lower than the SEB estimations during most rainy events. Nevertheless, despite possible measurement error accumulation when using the SEB method, time series are in very good agreement.
- The surface temperature dropped after each shower (as shown in Fig. 5), which largely reduced the upward long wave radiation from the asphalt, altering the radiation and energy balances, and enhancing the contribution of ground heat conduction which provided the necessary energy to evaporate the remaining water at the surface.

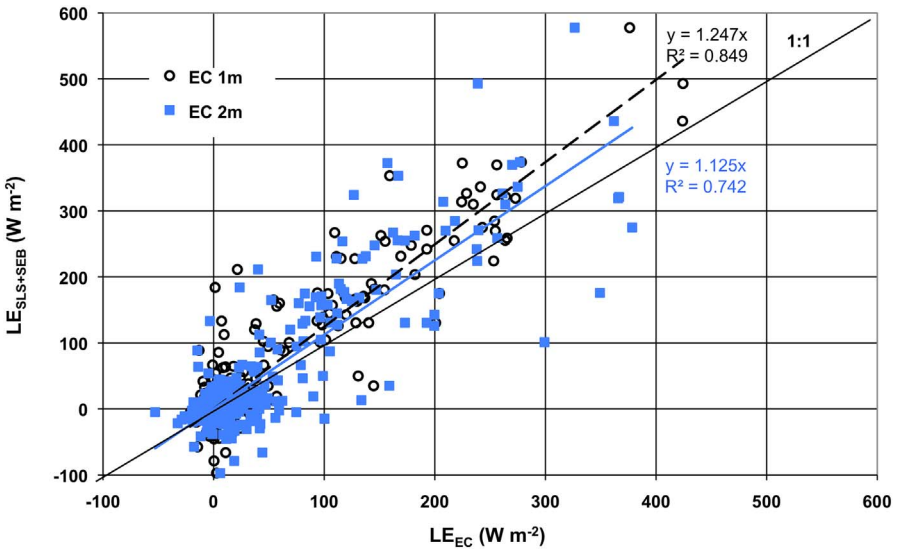

Fig. 9. Comparison of the latent heat flux estimation from the SEB residual method and the EC measurements at 1 m (black circles and dash line) and at 2 m (red squares and solid line). (For interpretation of the references to colour in this figure legend, the reader is referred to the web version of this article.)

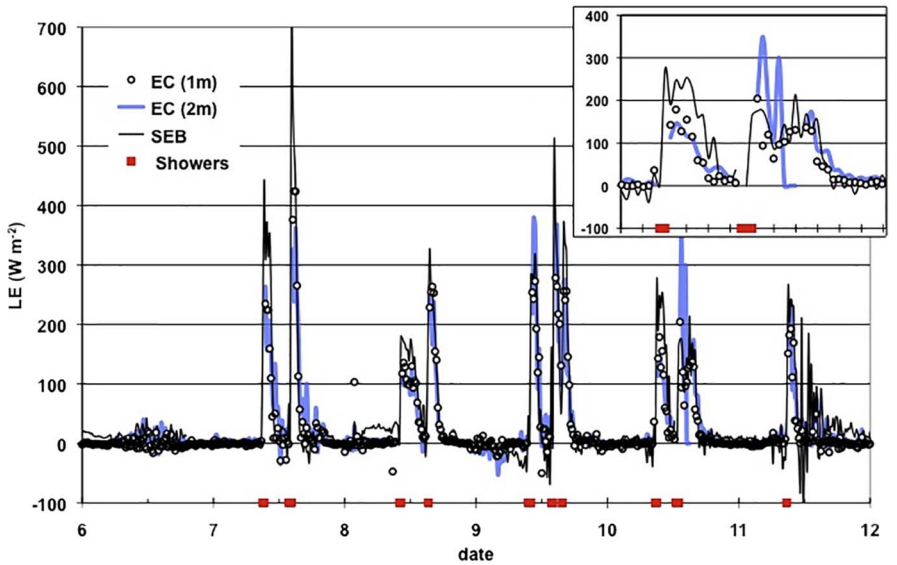

Fig. 10. Comparison of the latent heat flux estimated from the SEB residual using the scintillometer heat flux measurement and from the EC measurements at 1 m and at 2 m. The inset is a zoom on June 10 events from 06:00 UTC till 19:00 UTC.

- The uncertainty associated with the estimates of soil heat flux was assessed using night-time data: during the nights of June 6, 10 and 11, no turbulent fluxes were measured by the EC systems and the residual of the energy budget represented the uncertainty associated with $Rn - G$, which was lower than 20 W m^{-2}.
- During the June 7–8 night, the effect of a drizzle event was visible in the EC measurements at 1 m but not at 2 m showing that the near-neutral nocturnal condition hindered the vertical transfer between 1 and 2 m while the surface was still drying during several hours, as shown by the SEB estimation.
- Negative values were observed in the SEB residual time series at night-time and early morning of June 9. During that night, surface condensation might occur and negative flux values were also measured by the EC systems. However, we cannot explain the continuous decrease of the SEB residual in the morning which will require further investigation.
- In June 9 and 11, the residual from the SEB method shows strong alternations of positive and negative latent heat fluxes due to the very unsteady conditions during and after the rainfall events as it can be observed on Figs. 4 and 6. The different fluxes contributing to the SEB energy budget have different time constants, e.g. ~0.1 s for scintillometry heat flux and several minutes for ground heat flux. The derived latent heat may strongly fluctuate if the input fluxes, namely net radiation and ground heat flux, are not exactly in phase. More specifically, the harmonic method cannot reproduce rapid fluctuations of the surface temperature

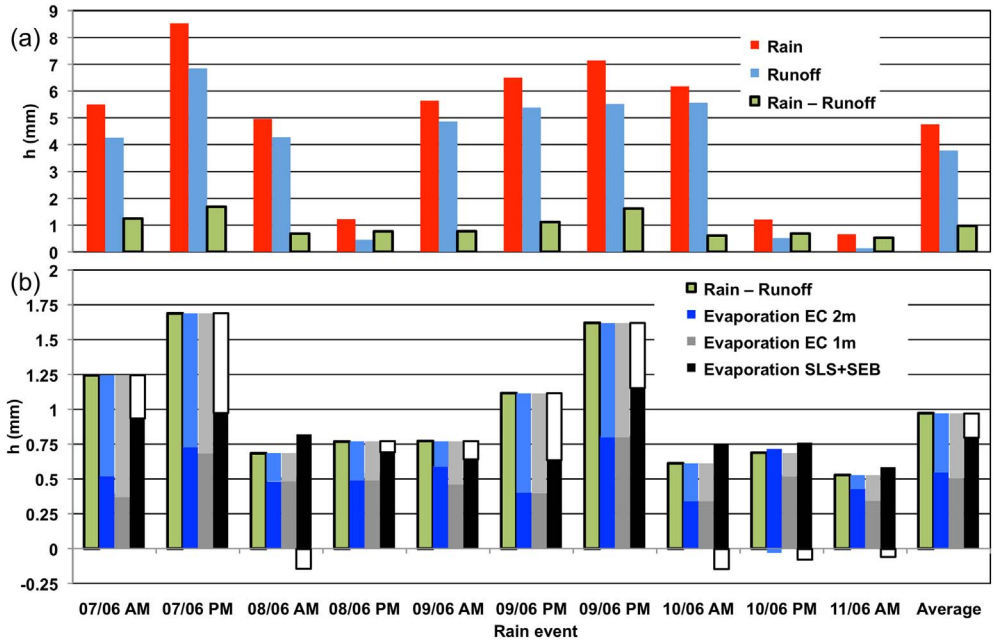

Fig. 11. Water budget of each rain event: (a) rain P, runoff R_R and the difference $P - R_R$, (b) $P - R_R$ (green bars), LE from the EC measurements and from the SEB residual (darker colours) and budget imbalance $I + X_W$ (lighter colours). (For interpretation of the references to colour in this figure legend, the reader is referred to the web version of this article.)

because they have been filtered out by diffusion processes in the temperature signal at $z_G = -1.5$ cm. It is also possible that the pyrgeometers had not enough time to dry up before successive showers, which might have slightly altered the SEB and the residual latent heat flux estimations.

5. Water budget results

The bulk water budget (Eq. (1)) was written for each specific rain event as follows for our experimental site; as $dh/dt = 0$ at this temporal scale:

$$P = R_R + (\rho_a L_w)^{-1} LE + I + X_w \tag{10}$$

where each of the components is the flux space and time integral over the instrumented square surface and the event duration (the brackets are omitted for simplicity). The evaporation rate is expressed from the cumulated latent heat flux and the residual term X_W expresses the eventual imbalance of the measured budget that may include water losses and measurement errors. The bulk water budget of each specific rain event was reported on Fig. 11 and expressed in equivalent water height h in mm.

The runoff is the main component of the bulk water budget and it represents on average 80% of the rain volume. The evaporation was deduced from the latent heat flux, either directly measured by the EC method or estimated from the SEB residual. One can see that the EC measurements with the KH2O hygrometers varied between 18 and 54% (33% in average) smaller volumes than the estimation with the SEB method using the scintillometer measurements, and the EC-based measurements at 2 m were 10% larger than the measurements at 1 m on average. Infiltration was not measured during the experiment. Ramier et al. (2011) monitored during 3 years two streets with similar asphalt concrete as our instrumented parking lot. Their tests with a double-ring infiltrometer yielded an infiltration capacity of approximately $3{\cdot}10^{-8}$ m s^{-1} while their analysis of the rainfall and runoff time series show that the infiltration rate may be estimated in the range 6–9 10^{-8} m s^{-1}, depending on the method or model. With these values the infiltration was estimated to remain between 0.1 and 0.2 mm during the artificial showers. However, the porosity of the parking lot asphalt concrete was very small. Therefore suction properties and initial dry conditions associated with the shortness of showers did not produce steady state infiltration. Thus during the transient period, infiltrated water was stored in the asphalt concrete layer close to the surface and removed by evaporation at the end of the showers. We conclude that the losses by deep infiltration were insignificant.

The bulk residual water volume was usually positive with EC measurements, except for the measurements at 2 m on June 10 PM (Fig. 11). Results confirm that EC measurements at low levels tend to underestimate the latent heat flux. The residual is lower with the SEB method but the average budget imbalance remains a water loss. The four events with a negative imbalance (Fig. 10) are those which occurred in cloudy conditions (Fig. 3), for which the SEB estimations of LE was on average larger than the EC measurements. Since R_R or P (Eq. (4)) are not linked with cloudy conditions, these imbalances are probably due to the estimation of LE from SEB. However, we are not able to conclude on the precise reason of these negative imbalances because they in the order of magnitude of the uncertainties associated with the SEB method which encompass both uncertainties on Rn-G ($\sim$20 W m^{-2}, see above 4.4.2) and

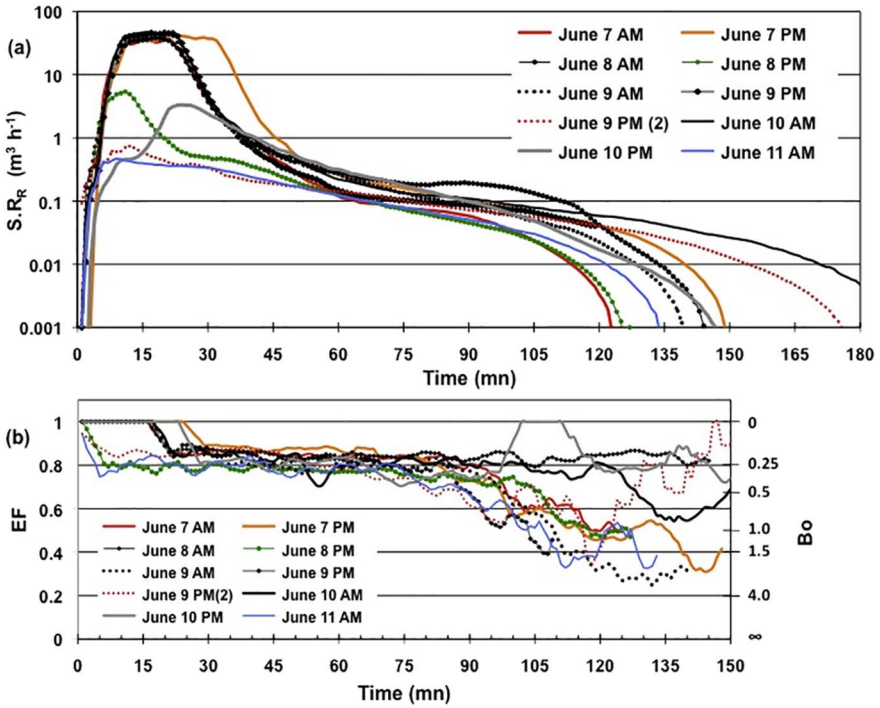

Fig. 12. Time series of the runoff flow rate in logarithmic scale (a) and of the evaporative fraction and Bowen ratio using the SEB method (b) during the rain events of June 7–11. The abscissa indicates the time from the start of the sprinklers. The numbers between brackets indicate shower duration (min).

uncertainties on H (~10% as estimated in Guyot (2010)).

The closure of the water budget $(P - R_R - (\rho_a L_w)^{-1} LE) / P$ was reached within 9–10% on average using the EC-based evaporation measurements and within 5% using the SEB method. These results could have probably been improved by accounting for infiltration. Assuming an infiltration flux of around 0.1–0.2 mm, as measured by Ramier et al. (2011) for a similar surface, would reduce the imbalance to about 8% and 4%, respectively.

6. Hydrological and energetic behaviour of asphalt surface during fair weather showers

Results showed the good performance of the SEB method using scintillometry-based sensible heat measurement to derive surface evaporation. The SEB method using scintillometry can also be used to monitor the rapid dynamics of the evaporation process which represent a significant advantage. Indeed, while the point-measurements with the EC method required a rather long integration time, the spatial averaging capacity of the scintillometer increased the statistical representativeness and provided fast variations of the sensible heat flux at the scale of one minute. Since the radiometers and the thermocouples in the ground also provided reliable measurements at 1-min temporal resolution, the SEB method was used to analyse runoff and latent heat flux fluctuations at 1-min time scale (Fig. 12).

The natural rainfall event captured on June 10 at 12:30 pm was associated with a total cumulative precipitation of 1.2 mm and a smaller precipitation rate than the sprinkler showers. For this event, the runoff water appeared to be released by the surface much later than for artificial showers because rain rate and infiltration rate became closer (Fig. 12a). For the simulated showers, the runoff started just a few minutes after the beginning of the rain and reached a steady regime after approximately 10 min. The steady regime lasted a few minutes after the end of the rain and then the flow decreased during 20 min, except for short-shower events (June 8 PM, 10 PM and 11 AM) for which the runoff started to decrease before the steady regime was reached. Then, a residual runoff regime further held out for at least one hour. It should be noted that during the afternoon of June 9, this residual regime did not influence the runoff of the following shower (PM2). A secondary maximum could be observed on the curves of June 8 and 11; it was certainly due to the asphalt topography and well visible during these two events with low incoming radiation conditions, hence with low evaporation rates, while it was not observed in more sunny conditions.

The evaporative fraction EF is defined as the ratio between the latent heat LE and the available energy at the surface for turbulent transfers:

$$EF = \frac{LE}{H + LE} = \frac{LE}{Rn - G - Q_R} \tag{11}$$

The evaporative fraction is related to the Bowen ratio $Bo = H / LE$ as:

$$EF^{-1} = Bo + 1 \quad (12)$$

Time series of the evaporative fraction were obtained from *H* measurements with the scintillometer and *LE* from the SEB residual at 1-min time step (Fig. 12b). During the rain the sensible heat flux was not measured and it was assumed null, yielding $EF = 1$. After each shower *EF* rapidly reached a value of 0.8 and it remained constant as long as the surface was wet, the runoff remaining around $100\ L\ h^{-1}$ ($3\ 10^{-5}\ m^3\ s^{-1}$). During the drying period under sunny conditions, the ground temperature generally increased (see Fig. 3) and *EF* decreased to zero in about one hour. For these events, the concomitant decrease of *EF* and runoff about 90 min after the shower end (Fig. 12) was associated with the apparition of dry patches on the parking lot. These dry areas caused local increases of surface temperature, an increase of the average sensible heat fluxes, and a slower runoff caused by longer pathways and an increased roughness within the micro-topography. For conditions of low radiation due to cloud passages (e.g. June 8 and 10) or successive events in a short period of time (June 9 afternoon), the evaporative fraction remained constant around 0.8 and the Bowen ratio around 0.25 during several hours, as long as the surface was wet. A Bowen ratio of 0.25 is typical of irrigated orchards or grass, and some sea surfaces, while the values measured several hours after the showers were between 0.5 and 2, typical values observed for moist grasslands and forests (Stull, 1988). These results indicate that the asphalt surface must be potentially viewed as a strongly evaporative surface during rainy periods.

7. Discussion

Several methods have been tested to measure or derive energy and water budget terms and verify budget closure. Some of these results are discussed below and put in perspective of modelling issues for urban canopies in surface models.

Concerning the energy budget, we compared two methods of assessing the radiative budget, with a net radiation sensor and with four radiometers measuring the downward and reflected individual solar and infrared components. Based on the selected instruments (Table 1) we showed that the latter method was more reliable. This is in agreement with recent studies reporting that net radiation from the four radiative components is more precise especially at night (Blonquist et al., 2009). This is of primary importance to minimize uncertainties for any method that relies on the energy balance and we recommend the use of such 4 component sensors. We also compared two methods of estimating the heat flux in the ground by conduction: the direct measurement with a ground heat plate and the measurements of thermocouples at several depths into the ground using an harmonic method based on the temperature decomposition in Fourier series. We showed that the latter method provided better estimates, in phase with other energy flux components. This method requires more analysis as it is based on spectral calculation and must be fed with continuous data series. Thus, following Heusinkveld et al. (2004), we highly recommend to use the harmonic method in any calculation of the available energy.

We compared sensible heat fluxes derived from a sonic anemo-thermometer (EC method) at two different heights and a small aperture scintillometer set over a 70 m transect. We clearly show that EC measurements are height–dependent despite frequency corrections associated with height. The differences are supposed to be associated with the footprint extension, demonstrating the difficulty of measuring turbulent fluxes on isolated parcels. This is particularly true in urban environment, which is a heterogeneous composition of homogenous small parcels (smaller than 1 ha) of different land uses (e.g. artificial or vegetated squares, green roofs,) whose impact on city energy budget should be evaluated. Finally, the comparisons of latent heat fluxes measured by EC systems (KH2O open-path hygrometer) and derived from the energy budget using sensible heat from scintillometry showed that the indirect method provided a better balance of the water budget; this statement is relevant with previous studies involving both methods applied to natural areas (Guyot et al., 2009; Samain et al., 2012).

The scintillometer provided estimates of the sensible heat flux integrated over a 70 m transect with a higher spatial representativeness than the point measurement provided by the EC method. Even at that parcel scale the scintillometer aggregated efficiently the heat fluxes from dry and wet patches on the parking lot. Therefore, the average surface evaporation derived from the SEB equation was also more representative of our site. However, the SEB method required highly reliable measurements/estimates of the other surface fluxes since the residual latent heat flux directly reflected the uncertainties of the other components of the energy budget. This method was used by Guyot et al. (2009 and 2012) to integrate the fluxes over heterogeneous land covers but it necessitated to measure the available energy of each land cover type included in the scintillometer footprint. This is not always possible, especially for urban canopies. At larger city scales, we favour the development of micro-wave scintillometry to evaluate directly the integrated latent heat flux (Ward et al., 2015).

We observed (Fig. 11a) that the cumulative evaporation of each rain event did not significantly vary from one event to the next, whereas the cumulative precipitation varied by a factor 7 without correlation between evaporation and precipitation volumes. This result supports the reservoir modelling approach, where (semi-)impervious surfaces store a rather thin volume of water provisionally available for evaporation, while most of the extra rain water is evacuated by runoff as soon as this reservoir is full. The estimated values for our 2500 m2 experimental asphalt square correspond to a maximum reservoir height of 0.8 mm on average (Fig. 11a).

Finally, the analysis of evaporation time series at the 1-min rate was used to identify some specific features of the asphalt surface behaviour during the drying periods. The duration of these periods varied from one to several hours depending on local meteorological conditions, and especially on the radiation. This demonstrated how rapid is asphalt response dynamics, that cannot be observed using EC measurements because of the required integration time. This also promotes the use of scintillometry for fast surface responses as shown by Van Kesteren et al. (2013).

8. Conclusion

In this article, we compared several methods to characterize the water and energy fluxes to/from an urban surface made of asphalt concrete pavement and to a bulk uncertainty estimate by evaluating the water and energy budget closure. The experimental site was a relatively open parking lot where a 2500 m^2 area was instrumented to monitor the surface fluxes during artificial rain events generated by a sprinkler system. Like most urban areas, the limited size of this measurement area raised technical and methodological problems that were thoroughly analysed. Nine simulated showers and one natural rain were monitored in different meteorological conditions, from overcast to very sunny. In our experiment, all components of the energy and water budgets were meticulously measured with high quality instruments, and we were able to close the water budget within a ± 8% accuracy for individual events and 5% on average. These very good results reflect the quality of our data set which is available to the scientific community on demand.

The scintillometry method using SEB has been shown to provide reliable sensible and latent heat flux time series at a 1-min time scale during the experiment that were used to characterize the rapid changes in the hydrological and energetic budgets of the asphalt surface. The evaporative fraction was constant at 0.8 during the first part of the drying periods, independently of the meteorological conditions. This value is equivalent to a Bowen ratio of 0.25, typical of highly evaporative surfaces like tropical rainforests and oceans, or (maybe) watered green roofs. This value often lasted for 1 to 3 h after the shower, period during which the surface evaporation was significantly active, yielding 80% of the turbulent fluxes to the atmosphere. It contributed, on average, to 17% of the water budget. Then it dropped to values close to zero at the end of the drying period in a few tens of minute. Runoff was the primary component of the water budget and represented around 80% of the total precipitation. The equivalent water reservoir height of the parking surface was 0.8 mm. In addition to this campaign mainly realized in sunny conditions, it would be valuable to conduct the same experiment in other meteorological conditions (cloudy or rainy days, in autumn or spring seasons), in order to evaluate the relevance of the methods with lower evaporation fluxes.

Urban canopies are definitely more complicated than one simple asphalt area. However since urban hydrological, climatological and meteorological models require improved parameterizations and data bases describing surface responses, the present dataset would be very useful to refine parameterizations of, e.g., tiling surface models. Also, this study demonstrated an efficient experimental approach using a scintillometer and the SEB to monitor an homogeneous urban surface in order to better understand and model the surface water and energy budgets at this scale. As scintillometry can be used over km-long path-lengths, it gives further opportunities to assess energy and water budgets at the scale of a city.

Acknowledgements

The authors thank Richard De Jeu from VU University Amsterdam (now at VanderSat) and Roland Vogt from Basel University for courtesy lend of the Small Aperture Scintillometer, Bernard Flahaut, Yves Lorin, David Ramier, Jean-Marc Rouaud and Michel Violleau for their help in the measurements, Frederic Penven and Geremy Panthou for their help in statistics.

Funding

The ROSURE (2001 − 2002) and HydroVille (2003-2004) projects were funded by the National Institute for Earth Sciences and Astronomy (INSU) of the Centre National de la Recherche Scientifique (CNRS) ECCO-PNRH #20.

Trade names and companies are given for the benefit of the reader and do not imply any endorsement of the product or company by the authors.

Appendix A. Derivation of SLS20 scintillometer measurements

The covariance B_{12} of the logarithm of the amplitude of the two received signals (1 and 2) may be expressed by:

$$B_{12} = 0.124\overline{C_n^2}K^{7/6}{L_{SLS}}^{11/6}f_B\left(\frac{l_0}{\sqrt{\lambda L_{SLS}}}, \frac{d}{\sqrt{\lambda L_{SLS}}}, \frac{D}{\sqrt{\lambda L_{SLS}}}\right) \quad (A.1)$$

where $\overline{C_n^2}$ is the path-averaged structure parameter of the air refractive index, $K = 2\pi/\lambda$ the transmitted signal wave number and λ its wavelength, L_{SLS} the path length and f_B a univocal function of the dissipation length l_0, the separation length between the two beams d, and the optical aperture D (Thiermann and Grassl, 1992). The symbol — indicates a path-averaged value.

The refractive index is a function of the thermo-dynamical state of air but, since the infrared signal propagation is only sensitive to temperature fluctuations (Moene, 2003), $\overline{C_n^2}$ is expressed as a function of the structure parameter for temperature $\overline{C_T^2}$:

$$\overline{C_T^2} = \left(\frac{T^2}{7.89\ 10^{-5}P_a}\right)^2\overline{C_n^2} \quad (A.2)$$

where P_a is the atmospheric surface pressure. Using Monin-Obukhov similarity theory $\overline{C_T^2}$ is related to the characteristic temperature scale $T_{SLS}{}^*$ for unstable conditions:

$$\overline{C_T^2}(\kappa z_{SLS})^{2/3}T_{SLS}^{*\,-2} = 4\beta_1(1 - 7z_{SLS}/L_{MO} + 75(z_{SLS}/L_{MO})^2)^{-1/3} \quad (A.3)$$

where L_{MO} is Obukhov length, z_{SLS} the beam height, κ and β_1 the Von Karman and Corsin constants, respectively. $T_{SLS}{}^*$ and L_{MO} are defined by:

$$T^*_{SLS} = \frac{\langle \overline{w'T'} \rangle}{u^*_{SLS}} = \frac{H_{SLS}}{\rho_a C p_a u^*_{SLS}} \tag{A.4}$$

$$L_{MO} = -\frac{g\kappa T^*_{SLS}}{z_{SLS} T u^{*2}_{SLS}} \tag{A.5}$$

The friction velocity $u_{SLS}{}^*$ is related to l_0 through its relationship with the dissipation rate of turbulent kinetic energy ε

$$\varepsilon k z_{SLS} u^{*-3}_{SLS} = (1 - 3z_{SLS}/L_{MO})^{-1} - z_{SLS}/L_{MO} \tag{A.6}$$

$$\varepsilon = \nu^3 (7.4/l_0)^4 \tag{A.7}$$

where ν is the viscosity of air. Thus $u_{SLS}{}^*$ and $T_{SLS}{}^*$ are obtained from an iterative computation of Eqs. (A.3)–(A.6), and the sensible heat flux H is further derived from Eq. (A.4).

References

Amato, F., Querol, X., Johansson, C., Nagl, C., Alastuey, A., 2010. A review on the effectiveness of street sweeping, washing and dust suppressants as urban PM control methods. Sci. Total Environ. 408 (16), 3070–3084.

Anandakumar, K., 1999. A study on the partition of net radiation into heat fluxes on a dry asphalt surface. Atmos. Environ. 33 (24–25), 3911–3918.

Aubinet, M., Vesala, T., Papale, D., 2012. Eddy Covariance: A Practical Guide to Measurement and Data Analysis (438 pp.). Springer.

Berthier, E., Andrieu, H., Rodriguez, F., 1999. The Rezé urban catchments database. Water Resour. Res. 35 (6), 1915–1919.

Berthier, E., Andrieu, H., Creutin, J.D., 2004. The role of soil in the generation of urban runoff: development and evaluation of a 2D model. J. Hydrol. 299 (3–4), 252–266.

Blonquist Jr., J.M., Tanner, B.D., Bugbee, B., 2009. Evaluation of measurement accuracy and comparison of two new and three traditional net radiometers. Agric. For. Meteorol. 149 (10), 1709–1721.

Braud, I., Noilhan, J., Bessemoulin, P., Mascart, P., Haverkamp, R., Vauclin, M., 1993. Bare-ground surface heat and water exchanges under dry conditions: observations and parameterization. Bound.-Layer Meteorol. 66 (1), 173–200.

Chadbourn, B.A., Luoma, J.A., Newcomb, D.E., Voller, V.R., 1996. Consideration of hot mix asphalt thermal properties during compaction. In: Quality Management of Hot Mix Asphalt. ASTM International.

Changnon, S.A., 1981. Metromex, a review and summary. In: Meterological Monographs. 18(40) Springer Link((http://link.springer.com/book/10.1007%2F978-1-935704-29-4) 181 pp.).

Christen, A., Vogt, R., 2004. Energy and radiation balance of a central European city. Int. J. Climatol. 24 (11), 1395–1421.

De Bruin, H.A.R., Meijninger, W.M.L., Smedman, A.-S., Magnusson, M., 2002. Displaced-beam small aperture scintillometer test. Part I: The Wintex Data-Set. Bound.-Layer Meteorol. 105 (1), 129–148.

Dupont, S., Mestayer, P.G., Guilloteau, E., Berthier, E., Andrieu, H., 2006. Parameterization of the urban water budget with the submesoscale soil model. J. Appl. Meteorol. Climatol. 45 (4), 624–648.

EdiRe http://www.geos.ed.ac.uk/homes/rclement/micromet/EdiRe/, Accessed date: 1 January 2017.

Foken, T., Wimmer, F., Mauder, M., Thomas, C., Liebethal, C., 2006. Some aspects of the energy balance closure problem. Atmos. Chem. Phys. 6 (12), 4395–4402. http://dx.doi.org/10.1007/978-94-007-2351-1_4.

Foken, T., Aubinet, M., Finnigan, J.J., Leclerc, M.Y., Mauder, M., Paw U, K.T., 2011. Results of a panel discussion about the energy balance closure correction for trace gases. Bull. Am. Meteorol. Soc. 92 (4), ES13–ES18.

Gash, J.H.C., Rosier, P.T.W., Ragab, R., 2008. A note on estimating urban roof runoff with a forest evaporation model. Hydrol. Process. 22 (8), 1230–1233.

Grimmond, C.S.B., Oke, T.R., 2002. Turbulent heat fluxes in urban areas: observations and a local-scale urban meteorological parameterization scheme (LUMPS). J. Appl. Meteorol. 41 (7), 792–810.

Grimmond, C.S.B., et al., 2010. The international urban energy balance models comparison project: first results from phase 1. J. Appl. Meteorol. Climatol. 49 (6), 1268–1292. http://dx.doi.org/10.1175/2010JAMC2354.1.

Grimmond, C.S.B., et al., 2011. Initial results from phase 2 of the international urban energy balance model comparison. Int. J. Climatol. 31 (2), 244–272. http://dx.doi.org/10.1002/joc.2227.

Guyot, A., 2010. Estimation de l'évapotranspiration sur un couvert complexe par utilisation de la scintillométrie infrarouge. Application à un bassin versant en zone soudano-sahélienne (Bénin). (Terre Univers Environnement. Grenoble, France, Université de Grenoble. PhD Thesis: 228 pp.).

Guyot, A., Cohard, J.-M., Anquetin, S., Galle, S., Lloyd, C.R., 2009. Combined analysis of energy and water balances to estimate latent heat flux of a sudanian small catchment. J. Hydrol. 375 (1–2), 227–240.

Guyot, A., Cohard, J.-M., Anquetin, S., Galle, S., 2012. Long-term observations of turbulent fluxes over heterogeneous vegetation using scintillometry and additional observations: a contribution to AMMA under Sudano-Sahelian climate. Agric. For. Meteorol. 154–155 (0), 84–98.

Hartogensis, O.K., De Bruin, H.A.R., Van De Wiel, B.J.H., 2002. Displaced-beam small aperture scintillometer test. Part II: cases-99 stable boundary-layer experiment. Bound.-Layer Meteorol. 105 (1), 149–176.

Hendel, M., Gutierrez, P., Colombert, M., Diab, Y., Royon, L., 2016. Measuring the effects of urban heat island mitigation techniques in the field: Application to the case of pavement-watering in Paris. Urban Clim. 16, 43–58. http://dx.doi.org/10.1016/j.uclim.2016.02.003.

Herb, W.R., Janke, B., Mohseni, O., Stefan, H.G., 2008. Thermal pollution of streams by runoff from paved surfaces. Hydrol. Process. 22 (7), 987–999.

Heusinkveld, B.G., Jacobs, A.F.G., Holtslag, A.A.M., Berkowicz, S.M., 2004. Surface energy balance closure in an arid region: role of soil heat flux. Agric. For. Meteorol. 122 (1–2), 21–37.

Hill, R.J., 1992. Review of optical scintillation methods of measuring the refractive-index spectrum, inner scale and surface fluxes. Waves Random Complex Media 2 (3), 179–201.

Hollis, G.E., Ovenden, J.C., 1988. The quantity of stormwater runoff from ten stretches of road, a car park and eight roofs in Hertfordshire, England during 1983. Hydrol. Process. 2 (3), 227–243.

Incropera, F.P., DeWitt, D.P., Bergman, T.L., Lavine, A.S., 2006. Fundamentals of Heat and Mass Transfer, 6th edition. John Wileys & Sons.

Kim, J.-Y., Sansalone, J.J., 2008. Zeta potential of clay-size particles in urban rainfall-runoff during hydrologic transport. J. Hydrol. 356 (1–2), 163–173.

Kinouchi, T., Kanda, M., Kuriki, M., Kobayashi, H., 1997. An observation of the climatic effect of watering on paved roads. J. Hydrosci. Hydraul. Eng. 15 (1), 55–64.

Lagouarde, J.-P., Irvine, M., Bonnefond, J., Grimmond, C., Long, N., Oke, T., Salmond, J., Offerle, B., 2006. Monitoring the sensible heat flux over urban areas using large aperture Scintillometry: case study of Marseille City during the Escompte experiment. Bound.-Layer Meteorol. 118 (3), 449–476.

Lemonsu, A., Masson, V., Berthier, E., 2007. Improvement of the hydrological component of an urban soil–vegetation–atmosphere–transfer model. Hydrol. Process. 21

(16), 2100–2111.
Mestayer, P.G., Durand, P., et al., 2005. The urban boundary-layer field campaign in Marseille (UBL/CLU-Escompte): set-up and first results. Bound.-Layer Meteorol. 114 (2), 315–365.
Mestayer, P., Rosant, J.-M., Rodriguez, F., Rouaud, J.-M., 2011. La campagne expérimentale FluxSAP 2010: Mesures de climatologie en zone urbaine hétérogène, La Météorologie. 73. pp. 34–44(English version in Urban Climate News (www.urban-climate.org) 40, 22-30).
Moene, A., 2003. Effects of water vapour on the structure parameter of the refractive index for near-infrared radiation. Bound.-Layer Meteorol. 107 (3), 635–653.
Mrawira, D.M., Luca, J., 2006. Effect of aggregate type, gradation, and compaction level on thermal properties of hot-mix asphalts. Can. J. Civ. Eng. 33 (11), 1410–1417.
Oke, T.R., 1979. Review of urban climatology 1973-1976. In: World Meteo. Organ. Technical Note N° 539.
Pigeon, G., Legain, D., Durand, P., Masson, V., 2007. Anthropogenic heat release in an old European agglomeration (Toulouse, France). Int. J. Climatol. 27 (14), 1969–1981.
Ragab, R., Bromley, J., Rosier, P., Cooper, J.D., Gash, J.H.C., 2003a. Experimental study of water fluxes in a residential area: 1. Rainfall, roof runoff and evaporation: the effect of slope and aspect. Hydrol. Process. 17 (12), 2409–2422.
Ragab, R., Rosier, P., Dixon, A., Bromley, J., Cooper, J.D., 2003b. Experimental study of water fluxes in a residential area: 2. Road infiltration, runoff and evaporation. Hydrol. Process. 17 (12), 2423–2437.
Ramamurthy, P., Bou-Zeid, E., 2014. Contribution of impervious surfaces to urban evaporation. Water Resour. Res. 50 (4), 2889–2902. http://dx.doi.org/10.1002/2013WR013909.
Ramier, D., Berthier, E., Andrieu, H., 2011. The hydrological behaviour of urban streets: long-term observations and modelling of runoff losses and rainfall–runoff transformation. Hydrol. Process. 25 (14), 2161–2178.
Rodriguez, F., Andrieu, H., Morena, F., 2008. A distributed hydrological model for urbanized areas - model development and application to case studies. J. Hydrol. 351 (3–4), 268–287.
Rotach, M.W., Vogt, R., et al., 2005. BUBBLE–an urban boundary layer meteorology project. Theor. Appl. Climatol. 81 (3), 231–261.
Rozoff, C.M., Cotton, W.R., Adegoke, J.O., 2003. Simulation of St. Louis, Missouri, Land Use Impacts on Thunderstorms. J. Appl. Meteorol. 42 (6), 716–738.
Samain, B., Simons, G.W.H., Voogt, M.P., Defloor, W., Bink, N.J., Pauwels, V., 2012. Consistency between hydrological model, large aperture scintillometer and remote sensing based evapotranspiration estimates for a heterogeneous catchment. Hydrol. Earth Syst. Sci. 16 (7), 2095–2107.
Santamouris, M., 2014. Cooling the cities – a review of reflective and green roof mitigation technologies to fight heat island and improve comfort in urban environments. Sol. Energy 103, 682–703.
Schmid, H.P., Oke, T.R., 1990. A model to estimate the source area contributing to turbulent exchange in the surface layer over patchy terrain. Q. J. R. Meteorol. Soc. 116 (494), 965–988.
Steffen, W., Broadgate, W., Deutsch, L., Gaffney, O., Ludwig, C., 2015. The trajectory of the Anthropocene: the great acceleration. Anthropocene Rev. 2 (1), 81–98.
Stull, R.B., 1988. An Introduction to Boundary Layer Meteorology. Kluwer Academic Pub, Dordrecht, The Netherlands (274 pp.).
Thielen, J., Wobrock, W., Gadian, A., Mestayer, P.G., Creutin, J.D., 2000. The possible influence of urban surfaces on rainfall development: a sensitivity study in 2D in the meso-γ-scale. Atmos. Res. 54 (1), 15–39. http://dx.doi.org/10.1016/S0169-8095(00)00041-7.
Thiermann, V., Grassl, H., 1992. The measurement of turbulent surface-layer fluxes by use of bichromatic scintillation. Bound.-Layer Meteorol. 58, 367–389.
Van Buren, M.A., Watt, W.E., Marsalek, J., Anderson, B.C., 2000. Thermal enhancement of stormwater runoff by paved surfaces. Water Res. 34 (4), 1359–1371.
Van Kesteren, B., Hartogensis, O.K., van Dinther, D., Moene, A.F., De Bruin, H.A.R., Holtslag, A.A.M., 2013. Measuring H2O and CO2 fluxes at field scales with scintillometry: part II – validation and application of 1-min flux estimates. Agric. For. Meteorol. 178–179, 88–105.
Van Wijk, W., De Vries, D., 1963. Periodic temperature variations in a homogeneous soil. In: van Wijk, W.R. (Ed.), Physics of Plant Environment. North-Holland Publishing Company, Amsterdam, The Netherlands, pp. 103–143.
Verhoef, A., 2004. Remote estimation of thermal inertia and soil heat flux for bare soil. Agric. For. Meteorol. 123 (3–4), 221–236.
Verhoef, A., van den Hurk, B.J.J.M., Jacobs, A.F.G., Heusinkveld, B.G., 1996. Thermal soil properties for vineyard (EFEDA-I) and savanna (HAPEX-Sahel) sites. Agric. For. Meteorol. 78 (1–2), 1–18.
Ward, H.C., Evans, J.G., Grimmond, C.S.B., 2015. Infrared and millimetre-wave scintillometry in the suburban environment - part 2: large-area sensible and latent heat fluxes. Atmos. Meas. Tech. 8 (3), 1407–1424.
Wheelon, A.D., 2003. Electromagnetic Scintillation: Volume 2, Weak Scattering. Cambridge University press (435 pp.).